

Functorial invariants for chaos topology from data

Denisse Sciamarella*

*Institut Franco-Argentin d'Études sur le Climat et ses Impacts (CNRS – IRD – CONICET – UBA)
(IRL 3351 IFAECI), C1428EGA Ciudad Autónoma de Buenos Aires, Argentina and
CNRS – Centre National de la Recherche Scientifique, 75016 Paris, France*

(Dated: April 27, 2026)

The templex is a topological object bridging homologies and templates for chaotic dynamics. This article places the templex within category theory, introducing a directed path algebra, an edge operator on directed paths, and an equivalence relation for directed cycles that is distinct from directed homologies. The resulting functorial invariants are of two kinds: abelian-group invariants, namely the homology groups, and semigroup invariants, namely the generatex semigroups. These invariants are separable through forgetful functors and constitute a robust framework for identifying tipping points, disambiguating physical mechanisms, and benchmarking data-driven models against observations or simulations. The formulation sets forth a non-metric criterion for chaos from finite-time data and reveals that the concatenable nature of Topological Modes of Variability is a direct consequence of the semigroup structure of the directed path algebra. The Rössler and Lorenz attractors are presented as paradigmatic examples, followed by the analysis of a climatic simulation and an experimental speech signal.

I. INTRODUCTION

Complex systems are governed by nonlinear dynamics exhibiting regimes, phases, transitions, tipping points, or extreme events. Despite the increasing abundance of data from observations and simulations, a persistent gap remains between what can be measured and the actual understanding of the main mechanisms governing the observed dynamics. Current approaches rely primarily on decompositions of the dynamics based on linear or statistical methods which struggle to capture the structural constraints imposed by the dynamics itself. This limitation is widely acknowledged in recent reviews, which emphasize the need for frameworks capable of bridging data-driven approaches with fundamental principles [1].

This bottleneck stems from the fact that the structure of a chaotic dynamical system cannot be robustly reconstructed without recourse to topological invariants [2, 3]. The Lorenz and Rössler chaotic attractors, for instance, exhibit nearly identical fractal dimensions, rendering them metrically indistinguishable under observational noise [4], in spite of their distinct organization in phase space. It is precisely this gap that chaos topology addresses: it provides a framework to link data to the principles governing trajectory organization in phase space. Under this paradigm, the topological characterization of flows becomes a central problem, relevant when validating reduced-order models, comparing observational sources, or assessing the topological consistency of models extracted via data-driven identification methods [5] as well as physics-informed machine learning [6].

Understanding chaotic dynamics from trajectory data has traditionally required two steps: reconstructing orbits in phase space, and then describing how they wind

around one another using braids, knots, or linking numbers [2, 7]. This information can be condensed in a so-called template or knot-holder. In a template, knotted orbits cycle around a joining chart where subsets of trajectories with different paths in phase space, called *strips*, merge together and share a common path before splitting apart again. This approach is effective in three dimensions for low-noise datasets, but becomes impractical as soon as orbits cannot be reliably recovered from point clouds, or in higher-dimensional dynamics, where knots generically unknot. Several attempts have explored how to extend templates beyond three dimensions, and move away from knot-based descriptions [8, 9].

A different approach bypasses orbit reconstruction altogether by working directly with the structure that supports a point set in phase space. This approach led to the construction of a cell complex in the sense of algebraic topology [10]. A cell complex is a scaffold composed of cells of layered dimensions, built in such a way that the topological invariants, i.e. properties that are preserved under homeomorphisms, can be extracted independently of the particular distribution or number of cells involved. Constructing cell complexes from point sets can be done following different rules, which will not necessarily yield a topologically faithful representation of the manifold supporting the underlying dynamics. Branched Manifold Analysis through Homologies [11, 12] assumes that the point set lies on a manifold which may have boundaries and branches, and builds a particular type of cell complex (now called the BraMAH complex) especially designed for this task [3, 13]. This framework allows one to compute homology groups (holes of different dimensions) of the supporting manifold, retaining generators and orientability properties. One can thus distinguish between spaces such as Möbius bands and cylinders, tori, Klein bottles, and pseudo-manifolds (such as branched manifolds).

Classical algebraic topology, however, describes only

* denisse.sciamarella@cnrs.fr

the structure of a space, without accounting for how that structure is actually visited by a flow. The domain that deals with the topology of directed spaces was born in the 1990s and is called directed algebraic topology [14–17]. To incorporate the directed organization of a flow in phase space, one must then move from traditional algebraic topology to directed algebraic topology. In parallel, when the goal is to describe chaotic attractors, one should move from a description in terms of BraMAH complexes to a description (which encompasses the latter) in terms of templexes [18–20]. A templex is a BraMAH cell complex endowed with a directed graph (digraph) whose nodes are the locally highest-dimensional cells (top-cells) and whose edges are the flow-compatible (directed) connections between these nodes.

The combination of both in a single object makes this digraph fundamentally different from those used in network analysis or clustering tools [21]. Because the digraph is tied to a cell complex, this structure allows for the extraction of invariants regardless of the specific segmentation of the point cloud, thus canceling out the scaffold’s extraneous information. The templex properties thus include the directionless invariants of classical topology mentioned above as well as the directed ones, called *stripexes*, since they extend the concept of strips in a template to higher-dimensional dynamics; for instance, the four strips of the classical Lorenz template correspond to four stripexes in the Lorenz templex. As we shall see, these directed invariants involve an equivalence relation that does not rely on topological voids. This distinction is central: while the undirected invariants describe the presence of holes, torsions or junction loci (the generalization of the joining chart), the directed invariants in a templex provide information about the specific type of chaotic organization at play.

Historically, the definition of cell complexes [22] and their associated homology preceded the advent of modern computational topology by several decades. This article follows the inverse path, providing a formal foundation for computational definitions of a templex and its properties [23]. This is achieved by leveraging the language of category theory [24, 25], which emerged in the 1940s as a technical tool in algebraic topology. The immediate problem was not the creation of a new foundational theory, but the need to formalize constructions that appeared repeatedly in topology. A category is defined by a collection of objects (e.g., spaces, groups) and arrows that represent morphisms between them (e.g., continuous maps, homomorphisms). A central notion in category theory is that of a *functor*, formalizing the idea that a construction in mathematics should respect the relations between objects, not just the objects themselves. For instance, the homology functor translates topological spaces into abelian groups. This shift of perspective allows one to identify common patterns across different areas of mathematics and to transfer results between seemingly unrelated contexts.

This article introduces several elements: a new type of

functor, an operator acting on finite formal concatenations of directed edges, and the quotient of directed cycles modulo the image of this operator. The algebraic structure that emerges for the directed invariants of a templex is that of a semigroup. The theory is illustrated with examples of two paradigmatic chaotic attractors [26, 27].

Finally, two applications are presented: a templex from an experimental speech example [11] is constructed for the first time, showing how the directed invariants enhance the homological description, and a recent application to non-autonomous climate dynamics is revisited, including the use of directed invariants to define the Topological Modes of Variability (TMVs). Previously introduced and extracted algorithmically [28], TMVs are here given a categorical formulation and a structural explanation for their non-superposable character.

The article concludes with a summary and an outline of how the functorial invariants can be interpreted in terms of the classical mechanisms organizing chaos in phase space, together with topological perspectives on the two application examples and, more generally, on nonlinear time series analysis and physics-informed machine learning.

II. THE TEMPLEX: DEFINITIONS

This section introduces mathematical definitions of the templex that generalize earlier constructions and place previously algorithmic procedures within a rigorous framework.

We first recall standard notions from homology theory. Next, we provide an intrinsic definition of a BraMAH complex. Finally, we describe how we incorporate flow-directionality.

A. Homologies

A *cell complex* is a topological space built by gluing cells of increasing dimension (points, segments, disks, and higher-dimensional analogues) along their boundaries. It provides a discrete, combinatorial representation of an underlying geometric object, and can be regarded as a topological scaffold: while the complex itself is not the object of interest, it supports algebraic constructions that reveal intrinsic properties of the space it represents. The dimension of a cell complex is defined as the highest dimension of its cells.

Given a finite cell complex K , the group of k -chains $C_k(K)$ is defined as the free abelian group generated by the k -cells of K ,

$$C_k(K) = \left\{ \sum_i n_i \sigma_i^k \mid n_i \in \mathbb{Z}, \sigma_i^k \text{ a } k\text{-cell of } K \right\},$$

together with a boundary operator

$$\partial_k : C_k(K) \longrightarrow C_{k-1}(K),$$

defined by assigning to each k -cell the formal sum of its $(k-1)$ -dimensional faces, with integer coefficients determined by their relative orientations.

The graded family of chain groups together with the boundary operators $\partial_k : C_k(K) \rightarrow C_{k-1}(K)$ that satisfy $\partial_{k-1} \circ \partial_k = 0$ is denoted by $C_\bullet(K) = \{C_k(K)\}_{k \geq 0}$. The group of k -cycles is the subgroup

$$Z_k(K) = \ker \partial_k \subset C_k(K),$$

while the group of k -boundaries is the subgroup

$$B_k(K) = \text{im } \partial_{k+1} \subset Z_k(K).$$

The k -th homology group is then defined as the quotient

$$H_k(K) = Z_k(K)/B_k(K).$$

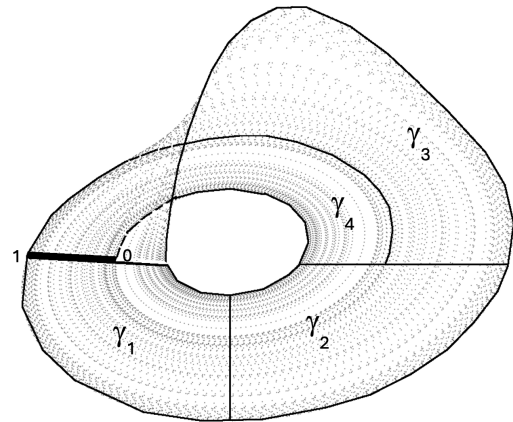
Intuitively, forming a quotient amounts to identifying objects that play the same structural role across different representations. A useful metaphor is that of musical notes: D3 and D4 are distinct pitches, separated by an octave, yet both belong to the same note class “D”, which might be known to some readers as “Re.” In homology, cycles that differ only by the attached higher-dimensional cells are identified in an analogous way, as they represent the same topological feature.

The generators of $H_k(K)$ correspond to intrinsic k -dimensional holes of the underlying space: they represent closed k -cycles that cannot be expressed as the boundary of any $(k+1)$ -dimensional chain. In this sense, homology detects topological features that are invariant under changes of the cell decomposition, capturing global properties such as connected components (0-holes), tunnels (1-holes), and higher-dimensional cavities ($k \geq 2$). A generator of $H_k(K)$ can be represented by any closed k -cycle within its equivalence class.

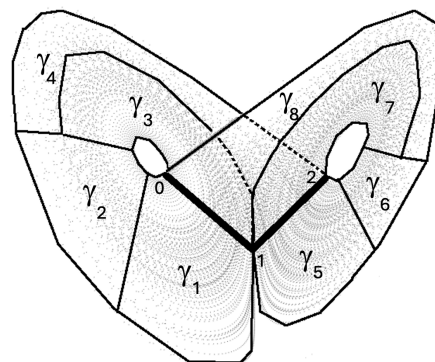
B. BraMAH complex

Cell complexes can be of different types depending on the construction rules used to build them from a point cloud. A BraMAH complex is designed so that the topology of a (branched) manifold underlying a point cloud in phase space can be faithfully described by a cell complex whose dimension coincides with that of the underlying manifold [11–13]. Here, a branched manifold is understood as a space that is locally a manifold almost everywhere [2].

In Ref. [19], a BraMAH complex of dimension h is defined as a cell complex constructed from a point cloud embedded in an n -dimensional phase space, with cells of dimension $k \leq h$, such that: (i) the 0-cells are a sparse subset of the original cloud of points in phase space; (ii) $h = d$, where $d \leq n$ is the intrinsic dimension of the underlying branched manifold being sampled; and (iii) each h -cell is such that h of the singular values that describe the distribution of the points around the barycenter of



(a) Rössler attractor



(b) Lorenz attractor

FIG. 1: BraMAH complexes K_R and K_L for two paradigmatic chaotic attractors, constructed with the minimum possible number of 2-cells. The 1-cells in the junction loci are indicated by thick lines: $\{\langle 0, 1 \rangle\}$ in (a) and $\{\langle 0, 1 \rangle, \langle 1, 2 \rangle\}$ in (b).

the cell scale linearly with the number of points in the cell [11, 12].

A BraMAH complex can be defined independently of algorithmic implementations as a finite cell complex K whose geometric realization $|K|$ is a manifold or a branched manifold, such that for each point $x \in |K|$ there exists an integer $\kappa(x)$ —the local topological dimension—for which a neighborhood of x is homeomorphic to an open subset of $\mathbb{R}^{\kappa(x)}$. A cell is said to be top-dimensional if it is not a face of any cell of strictly higher dimension in the complex, even if its dimension is not maximal globally. A *junction locus* is a subcomplex where three or more top-dimensional cells meet along cells of lower dimension, assuming a minimal local cell structure; see Ref. [18] for details. These are the loci where a branched manifold fails to be a manifold. Figures 1(a) and (b) display sampled trajectories and BraMAH complexes corresponding to two prototypical attractors. The junction loci are indicated with thick lines.

Computing homology groups for a BraMAH complex provides an algebraic translation of the topological properties of the structure of a possibly branched manifold sampled by a point cloud in phase space. The zeroth homology group H_0 detects the number of connected components of the sampled support, indicating whether the system explores a single connected region of phase space or several disconnected ones. For the attractors presented above, the flow evolves on a single structure without disjoint parts; therefore, both complexes consist of a single connected component, yielding $H_0(K_R) \cong \mathbb{Z}$ and $H_0(K_L) \cong \mathbb{Z}$.

Homology groups of degree $k \geq 1$ capture higher-dimensional features, corresponding to regions of phase space avoided by the data and translating into voids of the support [11–13, 29]. For K_R , the Rössler attractor complex in Fig. 1a, the boundary operator $\partial_2 : C_2(K_R) \rightarrow C_1(K_R)$ assigns to each 2-cell the signed sum of its boundary 1-cells. The operator $\partial_1 : C_1(K_R) \rightarrow C_0(K_R)$ acts on each oriented 1-cell $\langle i, j \rangle$ as

$$\partial_1 \langle i, j \rangle = \langle j \rangle - \langle i \rangle$$

One verifies that $\partial_1 \circ \partial_2 = 0$, as required. Computing kernels and images yields the homology groups

$$H_0(K_R) \cong \mathbb{Z}, \quad H_1(K_R) \cong \mathbb{Z}, \quad H_k(K_R) = 0 \text{ for } k \geq 2.$$

The single generator of $H_1(K_R)$ represents the central 1-dimensional void around which trajectories wind. Conversely, the symmetric butterfly-shaped structure of the Lorenz attractor presents two distinct central voids (one corresponding to each wing), thus resulting in two independent generators: $H_1(K_L) \cong \mathbb{Z}^2$.

Unlike constructions commonly used in persistent homology [30], the structure of a BraMAH complex does not depend on any filtration parameter. Top-cells can gather large subsets of points sampling the local topological structure of the manifold. This yields a topologically faithful cell complex, thus facilitating the computation of homology groups with integer coefficients, alongside the identification of extra structural features such as junction loci.

Betti numbers β_k , defined as the rank of the homology groups H_k , count the number of independent k -dimensional holes [10]. However, these homological ranks alone are insufficient to fully characterize the topology of the support; for instance, a cylinder and a Möbius band share identical Betti numbers. To resolve this degeneracy and detect the orientability properties of the complex, BraMAH evaluates the *orientability chain*, defined as the sum of the boundaries of all top-dimensional cells [12]. As illustrated in Table I, the evaluation of these chains provides the missing topological distinction, allowing one to rigorously discriminate between orientable and non-orientable manifolds.

TABLE I: Betti numbers β_k ($k = 0, 1, 2$) computed with integer coefficients and orientability properties for classic surfaces. A non-vanishing orientability chain indicates non-orientability, providing the necessary information to distinguish spaces with identical Betti numbers (e.g., the cylinder and the Möbius band) [12].

Cell complex	β_0	β_1	β_2	Orientability
Sphere (S^2)	1	0	1	Orientable
Cylinder	1	1	0	Orientable
Möbius band	1	1	0	Non-orientable
Torus (T^2)	1	2	1	Orientable
Klein bottle	1	1	0	Non-orientable

C. Templex

While homology captures the global structure of the set sampled in phase space, it is insensitive to temporal ordering. Let K be a BraMAH complex, and let

$$\mathcal{G} = (N, E)$$

be a directed graph, or *digraph*, whose nodes N correspond one-to-one with the top-cells of K , encoding the flow-compatible connections between them. The pair

$$\mathcal{T} = (K, \mathcal{G})$$

defines a *templex*. For the Rössler templex \mathcal{T}_R , the digraph \mathcal{G}_R consists of nodes $N_R = \{1, 2, 3, 4\}$ corresponding to the 2-cells $\{\gamma_1, \gamma_2, \gamma_3, \gamma_4\}$ and directed edges $E_R = \{(1, 2), (2, 3), (2, 4), (3, 1), (4, 1)\}$. In the Lorenz templex \mathcal{T}_L , the digraph \mathcal{G}_L has $N_L = \{1, \dots, 8\}$ from the eight 2-cells $\{\gamma_1, \dots, \gamma_8\}$, and directed edges $E_L = \{(1, 2), (2, 3), (2, 4), (3, 1), (4, 5), (5, 6), (6, 7), (7, 5), (6, 8), (8, 1)\}$.

A *subtemplex* of \mathcal{T} is a pair (K', \mathcal{G}') where $K' \subset K$ is a subcomplex and \mathcal{G}' is the subgraph of \mathcal{G} induced on the top-cells of K' . Once the digraph \mathcal{G} is taken into account, the junction locus, previously defined as a subcomplex of K , naturally induces a subtemplex of \mathcal{T} whose top-cells can be identified as *ingoing* or *outgoing* according to the direction of the flow across the lower-dimensional cell forming the junction. An *ingoing cell* (resp. *outgoing cell*) may therefore be referred to equivalently as an *ingoing node* (resp. *outgoing node*). Following the terminology introduced in template theory and used throughout previous works [18, 28], junction loci with a single ingoing node are called *splitting loci*, while those with a single outgoing node are called *joining loci*. For the Rössler templex \mathcal{T}_R , node 1 (γ_1) acts as an outgoing node (2-cell), receiving flow from ingoing nodes 3 and 4. In the Lorenz templex \mathcal{T}_L , there are two outgoing nodes 1 and 5, and four ingoing ones (3, 4, 7 and 8).

A *generatex* is a subtemplex whose subgraph is a directed cycle of \mathcal{G} . It is said to be of order p with $p \in \mathbb{N}$, $p \geq 1$, if the cycle has p distinct ingoing nodes. A generatex of order 1 is a *stripex* and a generatex of order $p > 1$

can be decomposed into p stripexes. Stripexes provide the direct bridge back to strips in the template tradition.

By construction, any simplex endowed with at least one joining locus necessarily contains intersections between its generatexes. For any subset of indices $\{i_1, \dots, i_m\}$ with $m \geq 2$, we define a *bond* as

$$B_{i_1 \dots i_m} = G_{i_1} \cap \dots \cap G_{i_m},$$

whenever this intersection is non-empty. The index set records precisely which generatexes share that portion of the dynamics, and the *valence* of the bond is m . The term *valence* refers to the analogy with valence electrons in chemistry, to emphasize that bonds encode how the fundamental dynamical units combine through the gluing of generatexes, in the same spirit as introduced in Ref. [20]. In the directed multigraph representation obtained from the union of generatexes, the valence of a given bond coincides exactly with the number of parallel edges along that subtemplex. Bonds with different index sets are distinct, even if they happen to share edges, as they encode different gluing relationships among the generatexes.

In \mathcal{T}_R , two generatexes are identified: $G_1 = \{1 \rightarrow 2 \rightarrow 3 \rightarrow 1\}$ and $G_2 = \{1 \rightarrow 2 \rightarrow 4 \rightarrow 1\}$. Their union forms a directed multigraph (Fig. 2a), where the single bond $B_{12} = G_1 \cap G_2 = \{1 \rightarrow 2\}$ has a valence of 2, evidenced by the two parallel edges connecting nodes 1 and 2. Similarly, \mathcal{T}_L presents three generatexes: $G_1 = \{1 \rightarrow 2 \rightarrow 3 \rightarrow 1\}$, $G_2 = \{5 \rightarrow 6 \rightarrow 7 \rightarrow 5\}$, and $G_3 = \{1 \rightarrow 2 \rightarrow 4 \rightarrow 5 \rightarrow 6 \rightarrow 8 \rightarrow 1\}$. Their intersection yields two distinct bonds: $B_{13} = G_1 \cap G_3 = \{1 \rightarrow 2\}$ and $B_{23} = G_2 \cap G_3 = \{5 \rightarrow 6\}$. Both bonds have a valence of 2, which corresponds to the pairs of parallel edges visible in the multigraph shown in Fig. 2b.

To see how the same result is obtained from templexes with a different number of 2-cells/nodes, please see Refs. [18, 19].

III. ALGEBRA OF DIRECTED PATHS

Following classical homology, this section develops an algebra of directed paths for a templex, conceived as the analogue of the algebra of chains for a cell complex.

A. Concatenation

Let $\mathcal{T} = (K, \mathcal{G})$ be a templex and let $C_{\mathcal{G}}(\mathcal{T})$ denote the set of all finite formal concatenations of directed edges of \mathcal{G} . Concatenation defines an associative product, so that for any three paths p, q, r ,

$$(pq)r = p(qr).$$

As direction matters in a templex, $C_{\mathcal{G}}(\mathcal{T})$ has the structure of a semigroup. For example, in \mathcal{T}_R , the directed edge $p = (3 \rightarrow 1)$ can be concatenated with $q = (1 \rightarrow 2)$

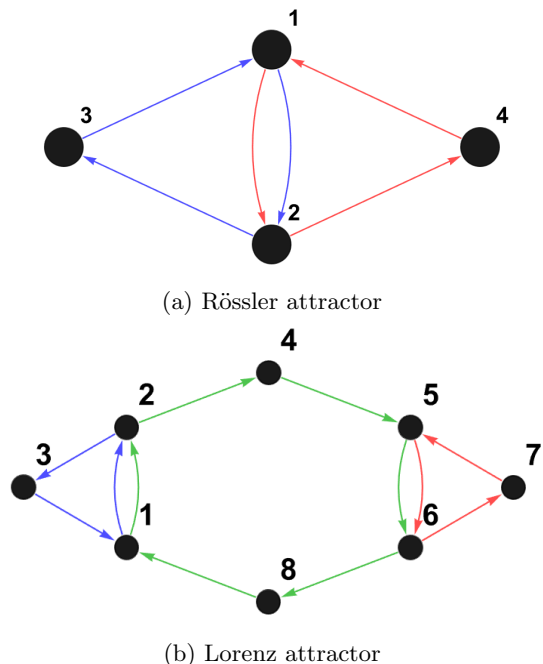


FIG. 2: Directed multigraphs for the Rössler and Lorenz templexes. Edges are colored according to the generatex they belong to. Parallel edges help identify bonds.

to form the path $pq = (3 \rightarrow 1 \rightarrow 2)$. However, the product qp is undefined, reflecting the irreversible nature of the flow.

B. Poincaré edges

Among the directed edges of a templex there are special ones: those connecting several ingoing nodes to a single outgoing node implicitly contain a lower-dimensional cell serving as frontier between those cells or nodes that are exclusive to a single generatex and those that belong to several generatexes. This lower-dimension cell constitutes the best location for Poincaré sections to compute strips with first return maps in template theory.

These key directed edges are hereafter called *Poincaré edges*. An individual Poincaré edge is denoted symbolically by a pair of ingoing and outgoing node labels,

$$\langle \text{ingoing node label} \mid \text{outgoing node label} \rangle,$$

and we denote by \bar{E} the set of all Poincaré edges of the templex \mathcal{T} . Notice that each joining locus (or each component of a joining locus as in the Lorenz case) gives rise to at least two Poincaré edges, reflecting the fact that the same outgoing top-cell/node is reached from two or more adjacent top-cells/nodes. The terminology is chosen to emphasize the role of these directed edges as transverse dynamical interfaces where distinct directed paths merge to become indistinguishable.

In the Rössler templex, there are two Poincaré edges: $\langle 3|1 \rangle$ and $\langle 4|1 \rangle$. Poincaré edges in the Lorenz templex are four: two of them ($\langle 3|1 \rangle$ and $\langle 8|1 \rangle$) associated with the first component of the junction (sharing 1-cell $\langle 0, 1 \rangle$), and the other two ($\langle 4|5 \rangle$ and $\langle 7|5 \rangle$) for the second component of the junction (sharing 1-cell $\langle 1, 2 \rangle$).

C. Poincaré-edge operator

The *Poincaré-edge operator* is defined as

$$\mathcal{P} : C_G(\mathcal{T}) \longrightarrow \bar{E}^*,$$

where \bar{E}^* denotes the set of all finite ordered sequences of Poincaré edges in \mathcal{T} .

Given a directed path p , the operator $\mathcal{P}(p)$ returns the ordered list of joining directed edges along p , in the order induced by the path, discarding all other directed edges. Thus, operationally, \mathcal{P} contracts a directed path onto the Poincaré edges it traverses. For directed cycles, this sequence is understood up to cyclic rotation.

Applying this operator to the generatexes of \mathcal{T}_R yields $\mathcal{P}(G_1) = \{\langle 3 | 1 \rangle\}$ and $\mathcal{P}(G_2) = \{\langle 4 | 1 \rangle\}$. For the Lorenz templex \mathcal{T}_L , one obtains $\mathcal{P}(G_1) = \{\langle 3 | 1 \rangle\}$, $\mathcal{P}(G_2) = \{\langle 7 | 5 \rangle\}$, and $\mathcal{P}(G_3) = \{\langle 4 | 5 \rangle, \langle 8 | 1 \rangle\}$, demonstrating how \mathcal{P} uniquely identifies the causal boundary sequence of each cycle.

D. Path templex

The *path templex* associated with a templex \mathcal{T} is the algebraic structure

$$T_\bullet(\mathcal{T}) = ((C_\bullet(K), \partial), (C_G(\mathcal{T}), \mathcal{P})),$$

where $C_\bullet(K)$ denotes the chain complex associated with a BraMAH complex K , and $C_G(\mathcal{T})$ denotes the collection of directed paths in the associated graph \mathcal{G} .

The notion of path templex introduced here should not be confused with that of a directed chain complex, nor with the dihomology framework developed in directed algebraic topology [14–17]. In the present construction, the underlying chain complex $C_\bullet(K)$ remains entirely classical: no causal direction is assigned to chains or to the boundary operator ∂ , and no homological theory is modified or replaced. Causality is encoded exclusively by directed paths and by the Poincaré-edge operator acting on them. The algebraization preserves a separation between the structure visited by the flow and the flow upon it, without decoupling them.

To illustrate $T_\bullet(\mathcal{T}_R)$, consider the BraMAH complex K_R introduced in Section II B. Following the notation of Munkres [31], the nonzero chain groups of $C_\bullet(K_R)$ are

$$\begin{aligned} C_2(K_R) &= \mathbb{Z}\langle \gamma_1, \gamma_2, \gamma_3, \gamma_4 \rangle, \\ C_1(K_R) &= \mathbb{Z}\langle \langle 0, 1 \rangle, e_1, e_2, \dots \rangle, \\ C_0(K_R) &= \mathbb{Z}\langle \langle 0 \rangle, \langle 1 \rangle, v_1, v_2, \dots \rangle, \end{aligned}$$

where $\langle 0, 1 \rangle$ denotes the junction 1-cell (Fig. 1a), and $\langle 0 \rangle, \langle 1 \rangle$ are its endpoint 0-cells. $C_G(\mathcal{T}_R)$ consists of all finite concatenations of these directed edges. For instance, $(3 \rightarrow 1) \cdot (1 \rightarrow 2) = (3 \rightarrow 1 \rightarrow 2)$ is a valid element, whereas the product $(1 \rightarrow 2) \cdot (3 \rightarrow 4)$ is undefined because node 3 does not connect to node 4 as a source. The path templex of the Rössler attractor is therefore

$$T_\bullet(\mathcal{T}_R) = ((C_\bullet(K_R), \partial), (C_G(\mathcal{T}_R), \mathcal{P})).$$

E. The generatex quotient

Let Z_G denote the set of directed cycles, i.e., of closed directed paths, in the digraph \mathcal{G} . Two directed cycles in \mathcal{G} are said to be equivalent if and only if they have the same image under the Poincaré-edge operator. This equivalence relation induces the quotient

$$\text{Gen}(\mathcal{T}) = Z_G / \sim,$$

whose elements are the *generatex classes*. By a standard abuse of notation, we will use the term *generatex* and the symbol G_i to denote both a specific directed cycle (the subtemplex) and its corresponding causal equivalence class in the semigroup.

This construction mirrors the classical algebraic-topological pipeline: directed paths play the role of chains, the Poincaré-edge operator extracts boundary-like causal information, and generatex classes arise as a quotient of directed cycles by this operator.

Back to the Rössler attractor, and since $\mathcal{P}(G_1) \neq \mathcal{P}(G_2)$, the two directed cycles belong to distinct equivalence classes in $Z_{\mathcal{G}_R} / \sim$. The classical chain complex encodes the single 1-hole of the Rössler branched manifold through $H_1(K_R) \cong \mathbb{Z}$, while the directed path algebra encodes, through the two generatex classes, the two non-equivalent ways of circling around the joining locus. Both levels of description are required: the hole is a directionless structural feature, whereas the two generatex classes are irreversible dynamical objects that cannot be detected by homology alone.

Notice that regular or quasiperiodic dynamics have no junction locus, hence no Poincaré edges: all directed cycles collapse into a single trivial equivalence class under \mathcal{P} , and the generatex semigroup reduces to the trivial semigroup. Conversely, a junction locus structurally forces the merging of at least two non-equivalent directed paths, yielding a non-trivial generatex semigroup.

A summary of the formal correspondences is provided in Table II, where X is a topological space and X^\uparrow a directed topological space.

F. Orientation-reversing and orientation-preserving classes

Let $\mathcal{T}_G = (K_G, \mathcal{G}_G)$ be the subtemplex defined by the union of all directed cycles belonging to a specific generatex class G .

Cell complex K	Templex $\mathcal{T} = (K, \mathcal{G})$
X	X^\uparrow
$C_\bullet(K)$	$C_\bullet(K), C_{\mathcal{G}}$
∂	∂, \mathcal{P}
$Z_k(K)$	$Z_k(K), Z_{\mathcal{G}}$
$H_k(K)$	$H_k(K), \text{Gen}(\mathcal{T})$

TABLE II: Algebraization of a cell complex and of a templex.

Assigning a consistent local orientation to each top-cell of K_G by propagating it across shared boundaries, the orientability chain is the sum of all their signed boundaries. A class G is *orientation-reversing* if any interior 1-cell appears in this chain with a coefficient of absolute value greater than 1; otherwise it is *orientation-preserving*.

In the Rössler case, studied via \mathcal{T}_R , the generatex class G_1 is orientation-preserving, whereas G_2 is orientation-reversing. When considered as isolated surfaces, G_1 is homeomorphic to a standard cylinder, while G_2 forms a Möbius band. In the Lorenz case, studied via \mathcal{T}_L , all three generatex classes are orientation-preserving.

IV. FUNCTORIAL INVARIANTS

The constructions introduced in the previous sections reveal two complementary levels in the description of dynamics: a structural one, captured by the topology of the underlying space, and a directional one, reflecting how this structure is effectively visited by the flow. This section addresses how both directionless and directed invariants can be related through a unified categorical perspective.

This correspondence is represented by the following commutative diagram, where the homology functor maps each chain complex to its homology groups:

$$\begin{array}{ccccc}
 \mathbf{Top} & \longrightarrow & \mathbf{Ch} & \longrightarrow & \mathbf{Ab} \\
 \\
 X & \longrightarrow & C_\bullet(X) & \longrightarrow & H_k(X) \\
 \downarrow & & \downarrow & & \downarrow \\
 Y & \longrightarrow & C_\bullet(Y) & \longrightarrow & H_k(Y)
 \end{array}$$

The category \mathbf{Ch} has graded abelian groups endowed with a boundary operator as objects, and degree-preserving morphisms commuting with the boundary operator as arrows.

In directed algebraic topology, the category \mathbf{dTop} consists of directed spaces and direction-preserving maps. In this setting, classical cell complexes and chain algebras are replaced by templexes and algebras of directed paths.

Let us denote by \mathbf{Pa} the category whose objects are directed path semigroups endowed with the Poincaré-edge operator, and whose morphisms are semigroup homomorphisms that send Poincaré edges to Poincaré edges.

A forgetful functor maps an object to a structure obtained by discarding part of the object's data, while keeping the remaining structure and the induced morphisms. Two forgetful functors arise naturally from the above commutative diagram.

The first one,

$$U_{\mathcal{G}} : \mathbf{dTop} \longrightarrow \mathbf{Ch},$$

forgets the digraph component and retains only the underlying chain complex, thereby recovering the classical functorial chain. The second one,

$$U_K : \mathbf{dTop} \longrightarrow \mathbf{Pa},$$

forgets the chain complex structure but preserves the directed path algebra together with the Poincaré-edge operator, which inherits properties derived from the prior construction of the BraMAH complex. It may seem a detail, but it is not: the inherited properties are being translated into the non-graded category \mathbf{Pa} . This feature is due to the fact that causal direction in the templex-based framework does not propagate to lower-dimensional cells, but remains confined to transitions between top-cells.

The categories \mathbf{Ch} and \mathbf{Pa} are scaffold-dependent. Functorial invariants must now condense the scaffold-independent properties. The generatex functor,

$$F_{Gen} : \mathbf{Pa} \longrightarrow \mathbf{Sem},$$

maps each path structure to the semigroup generated by its generatex classes. It plays for directed paths in a templex a role conceptually parallel to that played by the homology functor for chain complexes. The resulting composition,

$$F_{Gen} \circ U_K : \mathbf{dTop} \longrightarrow \mathbf{Sem},$$

defines a functorial construction parallel to the classical homology theory, but defining causal equivalence classes, and leading to a semigroup encoding its intrinsic directed invariants.

$$\begin{array}{ccccc}
 X^\uparrow & \longrightarrow & T_\bullet(X^\uparrow) & \longrightarrow & (H_k(X), \text{Gen}(X^\uparrow)) \\
 \downarrow & & \downarrow & & \downarrow \\
 Y^\uparrow & \longrightarrow & T_\bullet(Y^\uparrow) & \longrightarrow & (H_k(Y), \text{Gen}(Y^\uparrow))
 \end{array}$$

The new functorial chain sends directed spaces onto directed spaces, preserving the generatex structure with its associated Poincaré edges. It provides a functorial framework in which the classical directionless invariants, i.e.,

the homology groups, as well as the directed invariants, i.e., the generatex semigroups, coexist.

While homology group generators are classes of chains encircling voids in a topological space, generatex semigroups are classes of directed cycles circling around joining loci. The analogies between the two kinds of functorial invariants are summarized in Table III.

Level	Directionless	Directed
Spaces	Topological spaces $X \in \mathbf{Top}$	Directed spaces $X^\uparrow \in \mathbf{dTop}$
Algebraic encoding	Chain complex algebra $(C_\bullet, \partial) \in \mathbf{Ch}$	Directed path algebra $(C_G, \mathcal{P}) \in \mathbf{Pa}$
Algebraic invariants	Homology groups $H_k(X) \in \mathbf{Ab}$	Generatex semigroups $\text{Gen}(X^\uparrow) \in \mathbf{Sem}$

TABLE III: Categorical correspondences.

From a categorical perspective, a *pushout* provides a canonical way of gluing two algebraic structures along a common substructure. Accordingly, bonds between generatex classes admit a natural pushout interpretation. The bond $B_{i_1 \dots i_m}$ introduced in Section II C as a set-theoretic intersection of directed cycles is, under F_{Gen} , translated into an intersection of subsemigroups.

Let $\text{Gen}(X^\uparrow) \in \mathbf{Sem}$ denote the generatex semigroup associated with a directed space X^\uparrow . Given two generatex subsemigroups $G_1, G_2 \leq \text{Gen}(X^\uparrow)$, their *bond* is defined as the common subsemigroup

$$B_{12} = G_1 \cap G_2.$$

The canonical inclusions $B_{12} \hookrightarrow G_1$ and $B_{12} \hookrightarrow G_2$ define a cospan in \mathbf{Sem} , and hence a pushout diagram

$$\begin{array}{ccc}
 B_{12} & \xleftarrow{i_1} & G_1 \\
 \downarrow i_2 & & \downarrow j_1 \\
 G_2 & \xrightarrow{j_2} & G_1 \sqcup_{B_{12}} G_2
 \end{array} \quad (\text{in } \mathbf{Sem}),$$

which formalizes the gluing of generatex subsemigroups along their bond.

Within the functorial framework developed here, stripexes do not require a separate categorical treatment. They are elements of the generatex semigroup $\text{Gen}(\mathcal{T})$, and the generatex functor F_{Gen} maps them into \mathbf{Sem} . The distinction between stripexes and higher-order generatexes can be used to determine how many distinct subtrajectories can contribute to a single generatex class, but this does not alter the categorical structure. If generatexes are seen as the elementary building blocks of a chaotic dynamics, stripexes can be seen as the possibly non-cyclic components of a composite directed invariant.

The functorial invariants of the two paradigmatic attractors can now be read off directly from the path templex structure.

a. Rössler attractor Applying the forgetful functor U_G to \mathcal{T}_R recovers the classical chain complex $(C_\bullet(K_R), \partial)$, with $H_1(K_R) \cong \mathbb{Z}$ encoding the single central void. Applying U_K yields the directed path algebra $(C_G(\mathcal{T}_R), \mathcal{P})$, and the generatex functor F_{Gen} maps it to a semigroup with two generatex classes. The outer, orientation-reversing generatex class (G_2) is associated with Rössler's folding mechanism. It is worth noting that directed homology (dihomology), conceived to detect directed loops around topological voids, would not detect this mechanism. From a dihomological perspective, the Rössler branched manifold and a simple directed annulus (such as those arising from certain quasiperiodic flows) are equivalent, both enclosing a single 1-hole. The same applies to recurrence-based topological methods (e.g., cycling signatures from persistent homology [32]), which cannot separate the folding from the non-folding region.

b. Lorenz attractor The forgetful functor U_G recovers $H_1(K_L) \cong \mathbb{Z}^2$, reflecting the two central voids of the two wings. F_{Gen} yields a semigroup comprising three generatex classes. Two of them encompass the 1-holes, while the third one is of order 2, i.e. it contains two stripexes, one per wing. The bond structure is partial: the cross-wing generatex glues to the left-wing generatex along $B_{13} = \{1 \rightarrow 2\}$, and to the right-wing generatex along $B_{23} = \{5 \rightarrow 6\}$, while G_1 and G_2 share no bond. This captures the tearing mechanism around the saddle fixed point and gives two independent pushout diagrams,

$$\begin{array}{ccc}
 B_{13} & \xrightarrow{\quad} & G_1 \\
 \downarrow & & \downarrow \\
 G_3 & \xrightarrow{\quad} & G_1 \sqcup_{B_{13}} G_3
 \end{array}
 \quad
 \begin{array}{ccc}
 B_{23} & \xrightarrow{\quad} & G_2 \\
 \downarrow & & \downarrow \\
 G_3 & \xrightarrow{\quad} & G_2 \sqcup_{B_{23}} G_3
 \end{array}$$

both in \mathbf{Sem} .

The topological contrast between both attractors is clear and fully functorial: both attractors have bonds of valence 2, but Rössler has a single bond gluing its only two generatex classes, while Lorenz has two independent partial bonds, each connecting the cross-wing generatex class to one of the two lobe generatex classes.

V. DECOMPOSITION INTO TOPOLOGICAL MODES OF VARIABILITY

The functorial invariants introduced in Section IV are, by construction, metric-free: they describe equivalence classes of directed cycles, not the specific trajectories that realize them. A complementary, metric-level description is obtained by identifying the segments that correspond to each generatex class. This identification defines the *Topological Modes of Variability* (TMVs) introduced in Ref. [28]: a TMV consists of all trajectory segments that traverse the cells of a given generatex.

Let $\mathcal{T} = (K, \mathcal{G})$ be a templex and let $\text{Gen}(\mathcal{T}) = \{G_1, \dots, G_n\}$ be its set of generatex classes. A trajectory $\phi: [0, T] \rightarrow |K|$ induces a sequence of top-cell visits,

which can be read off from the digraph \mathcal{G} . We define a *generatex visitation label* of ϕ as a map

$$\chi : [0, T] \longrightarrow \{G_1, \dots, G_n\},$$

assigning to each instant t the generatex label carried by the trajectory at that time. For generatex classes of order $p > 1$, the trajectory may cross a joining locus and receive a new label before completing a full cycle, since each such crossing presents a new switching opportunity. The labeling $\chi(t)$ is therefore updated at each crossing of a joining locus (the lower-dimensional cell in K where the branched manifold fails to be a manifold) and remains constant between successive crossings.

When the trajectory enters a bond, it traverses cells that belong to several generatex classes simultaneously. The labeling χ does not become undefined or ambiguous in this region: the bond interval inherits the label of the specific generatex class the trajectory eventually resolves into.

The bond thus plays a twofold role. At the categorical level, it is a pushout object in **Sem** encoding the loss of causal distinguishability between generatex classes. At the metric level, however, the TMV decomposition cannot dispense with the cell complex K : it is precisely the crossing of the joining locus in K that triggers the label update and grounds the directed invariants in the geometry of the flow.

The generatex visitation label can be used to partition the time interval $[0, T]$ of (a set of) time series into a sequence of subintervals. The restriction of the trajectory to a subinterval labeled G_i is one *instance* of *TMV- i* . The full set of such subintervals, ordered in time, constitutes the *TMV decomposition* of the trajectory:

$$[0, T] = I_1 \cup I_2 \cup \dots \cup I_N, \quad \chi|_{I_k} = G_{\sigma(k)},$$

where $\sigma : \{1, \dots, N\} \rightarrow \{1, \dots, n\}$ is the sequence of generatex visits, and consecutive intervals are labeled by generatexes that are adjacent in the digraph \mathcal{G} .

This decomposition is *concatenable*: the subintervals are placed end to end in time, not superposed. This stands in direct contrast with linear-based modal decompositions (Fourier, Empirical Orthogonal Functions, Dynamic Mode Decomposition, Singular Spectrum Analysis), where modes are superposed at every instant. A TMV is active during a specific time interval and is then replaced by another. This is a direct consequence of the semigroup structure of the directed path algebra: concatenation, not superposition, is the natural operation on $C_{\mathcal{G}}(\mathcal{T})$.

The irregularity of the sequence σ and the variability of the lengths $|I_k|$ are metric manifestations of the directed invariants: an irregular sequence with variable residence times is the signature of chaotic dynamics switching among multiple generatex classes through joining loci.

The TMV decomposition can be illustrated on our two example attractors before turning to numerical and experimental data.

a. Rössler attractor Here, $\text{Gen}(\mathcal{T}_R) = \{G_1, G_2\}$ and the single joining locus is the 1-cell $\langle 0, 1 \rangle$ of K_R . Each crossing of this locus triggers a label update. The resulting sequence σ exhibits irregular alternation between the two generatex labels, with variable residence times $|I_k|$; see Fig. 3(a). The two generatex classes have an equal number of visits, namely 16 visits each, but markedly unequal residence times: the total time spent in G_1 is approximately 220 time units, with a mean visit duration of 14, while G_2 accumulates only 79 time units with a mean of 5. The asymmetry in residence times reflects the well-known geometry of the spiral Rössler attractor: trajectories wind slowly outward through many revolutions before reaching the fold, i.e., long visits in G_1 , and are then rapidly reinjected through the outer branch back to the inner spiral, i.e., short visits in G_2 . For this realization, the mean visit duration ratio $\langle |I|_{G_1} \rangle / \langle |I|_{G_2} \rangle \simeq 2.8$ captures the separation between the slow spiraling and the fast folding mechanism.

b. Lorenz attractor Here, $\text{Gen}(\mathcal{T}_L) = \{G_1, G_2, G_3\}$ with a two-component joining locus. A direct transition from G_1 to G_2 (or vice versa) is structurally forbidden. The cross-wing generatex class G_3 acts as a topological bridge: all transitions between the two lobe generatex classes are mediated by G_3 . This is a structural consequence of the partial bond structure and has no counterpart in classical modal decompositions. The resulting sequence σ is shown in Fig. 3(b). The left-wing G_1 and right-wing G_2 each record 26 visits, while the cross-wing class G_3 records $51 = 26 + 25$ visits, accumulating the largest total time (82.8 time units). For this specific realization, the mean residence times per visit are $\langle |I|_{G_1} \rangle = 1.7$, $\langle |I|_{G_2} \rangle = 2.4$, and $\langle |I|_{G_3} \rangle = 1.6$. The disparity between the two wings exemplifies how a symmetry in the governing equations does not preclude asymmetries in the residence times of finite-time realizations evaluated over a topological partition.

It is interesting that analogous asymmetries in residence times between alternating regimes of a system exist, for instance, in climate and weather variability. Thus, the well-known El Niño-Southern Oscillation phenomenon in the tropical Pacific has longer and fewer El Niño vs. La Niña episodes, where the time units are years [33]. The blocking vs. zonal flow variability in the Northern Hemisphere midlatitudes has the same asymmetry, but the time units are weeks [34].

VI. APPLICATIONS

Two case studies are provided to illustrate how the functorial invariants emerge from experimental [11] and numerical [28] data.

The first example is a speech signal previously used to show that the topology of short and noisy time series can actually be retrieved through homologies [11]. The templex and its directed invariants for this dataset are computed here for the first time. While the correspon-

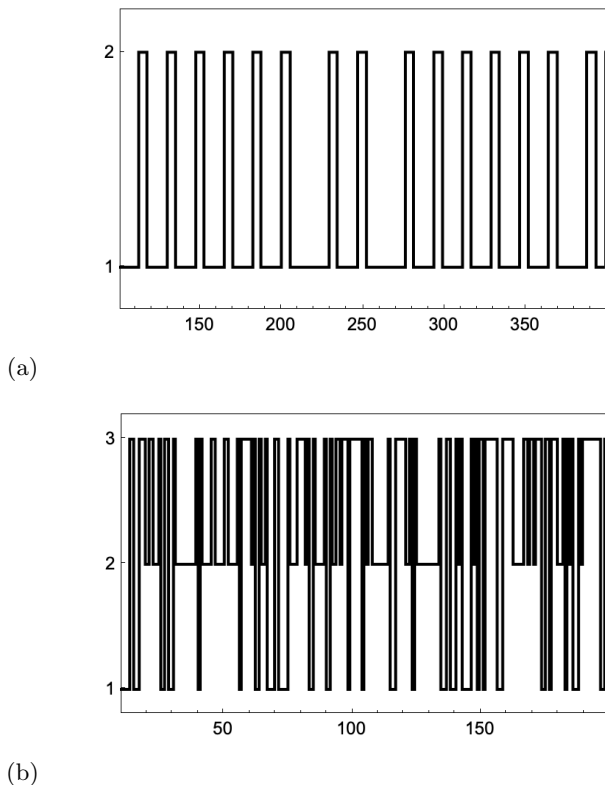


FIG. 3: Generatex visitation sequence for (a) the Rössler and (b) the Lorenz attractors.

dence between the embedded trajectory and a three 1-hole structure cannot be taken as an indication of chaos, the directed invariants obtained through the generatex functor can, as shown below.

The second example is a numerical simulation of a conceptual four-dimensional model that captures key processes of the large-scale ocean circulation [28]. This system is revisited to illustrate how functorial invariants can be handled in nonautonomous settings. The TMVs introduced in this setting as metric manifestations of generatexes can be used in the detection of the *topological tipping points (TTPs)* found in Ref. [35].

A. A speech signal

The speech signal analyzed here corresponds to pressure fluctuations generated by the airflow through the vocal folds during vowel production.

Vowel sounds result from a self-sustained oscillatory regime in which vocal-fold motion couples with the airflow driven by subglottal pressure. The vowel quality is further shaped by the supraglottal vocal tract, which acts as an acoustic resonator. The governing equations are inherently nonlinear, involve delayed feedback mechanisms, and are therefore known to produce complex and sometimes chaotic dynamical signatures.

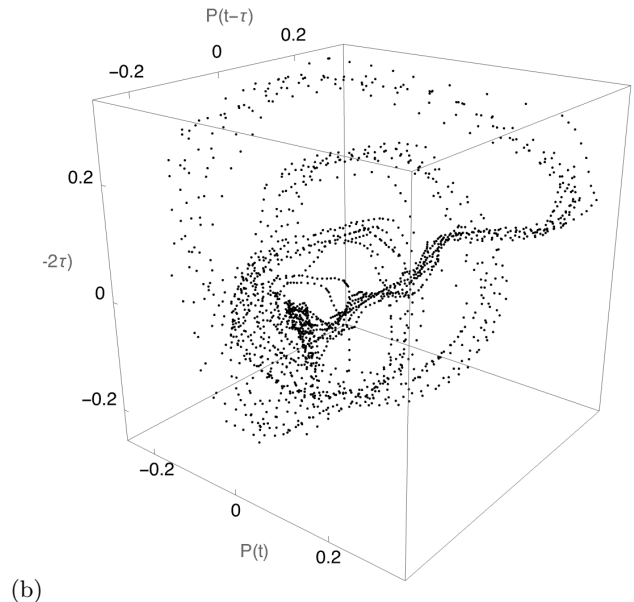
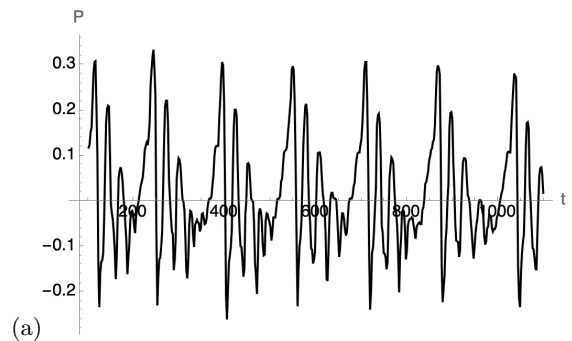


FIG. 4: The time series of the pressure fluctuation values (in arbitrary units) as a function of their position in the data file. (a) The entire time series for $t = 0.147$ sec. (b) The three-dimensional time-delay embedding of the time series, with $\tau = 5$.

Here we reconsider the dataset in Ref. [11], namely, the signal for vowel /a/ as pronounced in Spanish. The time series and its time-delay embedding are displayed in Figs. 4(a,b). The file contains 1183 points corresponding to a total interval of $t \approx 0.147$ s, with the measurements recorded at 8 000 samples per second. The BraMAH complex is reconstructed, so the number of 2-cells, their distribution, and labels differ from those in Ref. [11]. As expected, the homological features (three 1-holes) remain identical to those originally reported. This is a natural consequence of the formalism: the homology functor leads to invariants that are independent of the specific cell decomposition.

The analysis is conducted by applying the forgetful functor U_K , since homological properties were already discussed. The new aspect of the present work lies in the directed algebraic topology, which reveals three distinct generatex classes circling around two joining loci,

indicated by thick black lines in Fig. 5(a).

Each generatex is expressed as a cycle of the digraph, whose node indices correspond to the labels of point subsets forming 2-cells:

$$\begin{aligned} G_1 &= \{7 \rightarrow 17 \rightarrow 9 \rightarrow 18 \rightarrow 20 \rightarrow 21 \rightarrow 15 \rightarrow 16 \rightarrow 7\}, \\ G_2 &= \{7 \rightarrow 17 \rightarrow 9 \rightarrow 10 \rightarrow 11 \rightarrow 13 \rightarrow 14 \rightarrow 15 \\ &\quad \rightarrow 16 \rightarrow 7\}, \\ G_3 &= \{1 \rightarrow 2 \rightarrow 3 \rightarrow 4 \rightarrow 5 \rightarrow 6 \rightarrow 7 \rightarrow 17 \rightarrow 9 \\ &\quad \rightarrow 22 \rightarrow 23 \rightarrow 25 \rightarrow 19 \rightarrow 12 \rightarrow 1\}. \end{aligned}$$

G_1 and G_3 are orientation-reversing while G_2 is orientation-preserving. The bonds, given by:

$$\begin{aligned} B_{123} &= G_1 \cap G_2 \cap G_3 = \{7 \rightarrow 17 \rightarrow 9\}, \\ B_{12} &= G_1 \cap G_2 = \{15 \rightarrow 16 \rightarrow 7\}. \end{aligned}$$

can be identified in the digraph; see Fig. 5(b). Their valences are 3 in B_{123} and 2 in B_{12} .

To make the causal boundaries underlying these directed cycles explicit, we apply the Poincaré-edge operator \mathcal{P} to each generatex:

$$\begin{aligned} \mathcal{P}(G_1) &= \{\langle 21 | 15 \rangle, \langle 16 | 7 \rangle\}, \\ \mathcal{P}(G_2) &= \{\langle 14 | 15 \rangle, \langle 16 | 7 \rangle\}, \\ \mathcal{P}(G_3) &= \{\langle 6 | 7 \rangle\}. \end{aligned}$$

The two joining loci can be identified through the Poincaré edges that traverse them: $\langle 14 | 15 \rangle$ and $\langle 21 | 15 \rangle$ are associated with the first locus, while $\langle 16 | 7 \rangle$ and $\langle 6 | 7 \rangle$ correspond to the second. The generatex classes are thus connected through a double bond, which transitions into a triple bond when the respective directed paths re-inject into node 7. Each generatex class can be associated with a 1-hole, yielding branches separated by voids. This contrasts with the Rössler attractor, where folding occurs without creating an internal void between the bonded generatex classes.

Fig. 5(c) shows the visited generatex labels as a function of time, defined as $\chi(t)$ in Section V, that is, the itinerary induced by the dynamics on the TMV decomposition of the templex. The signal alternates irregularly between the three generatexes G_1, G_2, G_3 , with strongly variable residence times: approximately 320 time units in G_1 , 130 in G_2 , and 514 in G_3 . While transitions $G_3 \rightarrow G_1$ and self-concatenations $G_1 \rightarrow G_1$ dominate, the sequence $G_3 \rightarrow G_2 \rightarrow G_1$ appears only intermittently. This itinerant behavior across distinct orientation-reversing and orientation-preserving generatex classes provides a topological signature of the underlying vocal-fold dynamics.

B. Wind-driven double gyre

Understanding the effects of time-dependent forcing on intrinsic ocean variability is crucial for modeling climate variability in general. This section presents a numerical

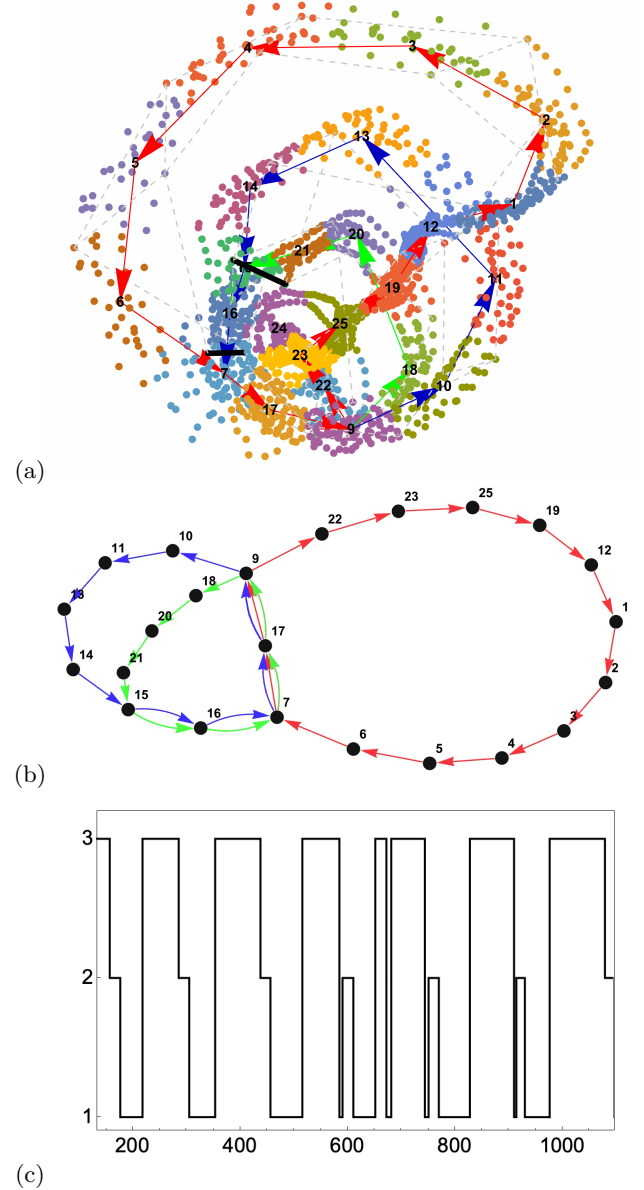


FIG. 5: Forgetful functor analysis of the time series in Fig. 4. (a) Point cloud segmented into the 2-cells of the BraMAH complex (1-cell boundaries shown as light-gray dashed lines). The two joining loci are indicated by thick black lines. (b) Directed multigraph obtained as the union of the three generatexes G_1 in green, G_2 in blue, and G_3 in red; parallel edges indicate bonds—the triple one B_{123} and the double one B_{12} . Removing parallel edges yields the digraph of the templex. (c) Generatex visitation sequence extracted from the time series [μsec].

simulation reported in Ref. [28] based on a model of intermediate complexity [34] for the streamfunction of the wind-driven ocean circulation in midlatitudes [36].

In the case of aperiodic wind-stress forcing, three junction loci (one joining locus and two splitting loci) are de-

tected. Note that top-cells are renumbered here as $\gamma_i \mapsto i$ ($i = 1, \dots, 6$) and $\sigma_j \mapsto 6 + j$ ($j = 1, \dots, 16$).

Six generatex classes are identified:

$$\begin{aligned} G_1 &= \{1 \rightarrow 2 \rightarrow 3 \rightarrow 4 \rightarrow 1\}, \\ G_2 &= \{1 \rightarrow 2 \rightarrow 3 \rightarrow 5 \rightarrow 6 \rightarrow 17 \rightarrow 18 \rightarrow 19 \\ &\quad \rightarrow 20 \rightarrow 21 \rightarrow 22 \rightarrow 1\}, \\ G_3 &= \{1 \rightarrow 2 \rightarrow 3 \rightarrow 5 \rightarrow 6 \rightarrow 12 \rightarrow 13 \rightarrow 1\}, \\ G_4 &= \{1 \rightarrow 2 \rightarrow 3 \rightarrow 5 \rightarrow 6 \rightarrow 7 \rightarrow 8 \rightarrow 1\}, \\ G_5 &= \{1 \rightarrow 2 \rightarrow 3 \rightarrow 5 \rightarrow 6 \rightarrow 9 \rightarrow 10 \rightarrow 11 \rightarrow 1\}, \\ G_6 &= \{1 \rightarrow 2 \rightarrow 3 \rightarrow 5 \rightarrow 6 \rightarrow 14 \rightarrow 15 \rightarrow 16 \rightarrow 1\}. \end{aligned}$$

Only G_2 and G_6 are orientation-reversing.

The directed multigraph is shown in Fig. 6(a). There are two bonds:

$$\begin{aligned} B_{123456} &= \bigcap_{i=1}^6 G_i = \{1 \rightarrow 2 \rightarrow 3\}, \\ B_{23456} &= \bigcap_{i=2}^6 G_i = \{1 \rightarrow 2 \rightarrow 3 \rightarrow 5 \rightarrow 6\}. \end{aligned}$$

The valence of the bonds, given by the number of parallel edges, is 6 for B_{123456} and 5 for B_{23456} . Applying the Poincaré-edge operator \mathcal{P} to each generatex, we obtain:

$$\begin{aligned} \mathcal{P}(G_1) &= \{\langle 4 \mid 1 \rangle\}, & \mathcal{P}(G_2) &= \{\langle 22 \mid 1 \rangle\}, \\ \mathcal{P}(G_3) &= \{\langle 13 \mid 1 \rangle\}, & \mathcal{P}(G_4) &= \{\langle 8 \mid 1 \rangle\}, \\ \mathcal{P}(G_5) &= \{\langle 11 \mid 1 \rangle\}, & \mathcal{P}(G_6) &= \{\langle 16 \mid 1 \rangle\}. \end{aligned}$$

The joining locus being traversed is given by the 1-cell labeled $[0, 1]$ in Fig. 14(a) of Ref. [28].

The generatex visitation label $\chi(t)$ defined in Section V is shown as a function of time in Fig. 6(b). The sequence σ exhibits irregular switching among the six generatexes, with variable residence times $|I_k|$. Notice that during the first 150 years the set of active TMVs consists of three generatex classes. The period starting subsequently includes two new generatex classes (number 1 and number 5). The sixth generatex class appears towards the end of the inspected time series. Physically, the emergence (or disappearance) of generatex classes translates into the forcing-dependent accessibility of macroscopic flow configurations and provides a characterization of topological tipping phenomena in nonautonomous settings [36, 37]. In this respect, the speech example presents no tipping and is therefore closer to the periodically forced case of the wind-driven double gyre, where the set of TMVs remains the same over the whole time window.

VII. SUMMARY AND CONCLUSIONS

The study of chaotic dynamics through topology is a program that can be formally broken into two parts: (i) the construction of the topological object from data, a task that pertains to computational topology; and (ii)

the algebraic handling of this object, which falls under algebraic topology. This article deals with (ii), assuming that (i) is adequately accomplished.

Branched Manifold Analysis through Homologies (BraMAH) builds on the template legacy by introducing a specific type of cell complex that allows extracting homology group generators, orientability chains, and junction loci from multi-dimensional point clouds obtained from discretely sampled time series. Instead of translating trajectories into Conway polynomials or linking numbers, BraMAH translates point clouds in arbitrary dimensions into topological invariants borrowed from homology theory.

Classical algebraic topology, however, treats structures as freely traversable in all directions. When point clouds arise from phase-space trajectories, time is implicit but present. The top-cells of a BraMAH complex therefore represent groups of visited states that are causally connected by the dynamics that generated the point cloud. The structure to be described is thus a directed space, or more precisely a directed subspace of phase space, which may have boundaries and non-manifold loci.

The templex is a topological object that is designed to capture both the classical algebraic topology and the directed algebraic topology of chaos. Category theory provides the formal way of translating a topological problem into an algebraic one, thanks to functors. Placing the templex within this formalism has required providing an intrinsic definition of a BraMAH complex, an algebra of directed paths, an edge operator and its associated quotient. The result is a formal setting with two complementary levels of information carried by the functorial invariants and separable through forgetful functors.

- **Undirected level (Homology groups):** It describes the structural scaffold with its voids and orientability properties. These invariants allow one to distinguish, for instance, an underlying torus from other supporting shapes, regardless of the sequence in which regions are visited. If the scaffold corresponds to a pseudo-manifold, BraMAH detects and locates the junction loci.
- **Directed level (Generatex semigroups):** It captures the irreversible causal organization around joining loci, if they exist. These invariants are obtained through a directed algebra of paths, providing information about the specific type of chaotic dynamics at play.

The classical mechanisms of chaotic phase-space organization naturally translate into this functorial framework:

- **Squeezing** is algebraically mapped to bonds which embody the topological overlap of distinct generatex classes; they are the regions where different futures are glued together, so that causal distinguishability is locally lost.

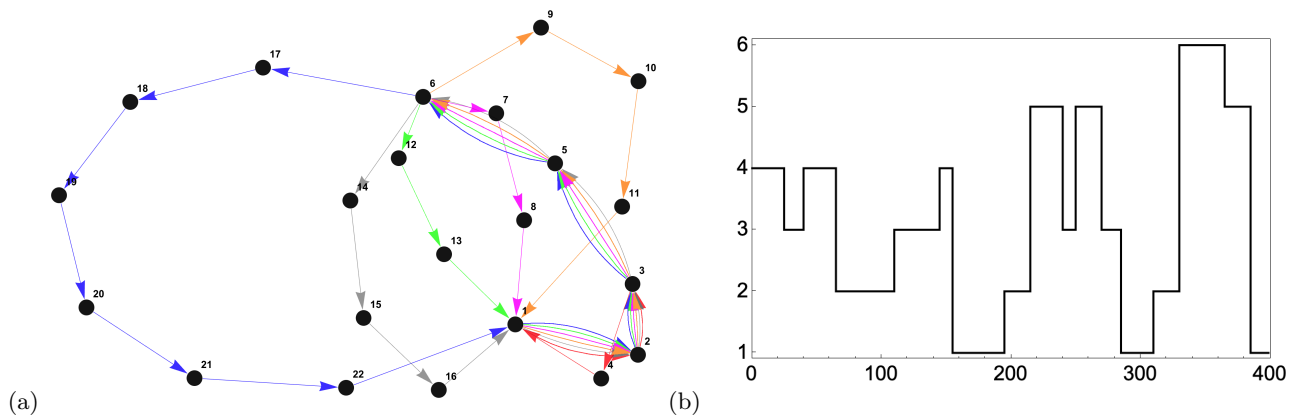


FIG. 6: (a) Directed multigraph obtained as the union of the six generatexes in red, blue, green, magenta, orange and gray for the templex of the aperiodically forced wind-driven double gyre example. (b) Generatex visiting sequence extracted from the time series (in years) of an individual solution, shown in Fig. 15 of Ref. [28].

- **Stretching** corresponds to the divergence of trajectories as they exit a bond and split into the distinct unbonded regions of their respective generatex classes, with the valence quantifying the number of non-equivalent directed paths available.
- **Folding** manifests as an orientation-reversing generatex class, captured by inspection of the orientability properties of each generatex studied as an independent and uniformly reoriented cell complex. Folding can occur with or without creating internal voids.
- **Tearing** actively splits the flow, typically segregating generatex classes and organizing them through different bonds, as observed in the Lorenz attractor. Tearing is absent in the Rössler case, which presents folding without tearing.

One must beware that topological voids do not necessarily imply tearing; a quasi-periodic toroidal dynamics possesses two 1-holes and one 2-hole but exhibits no tearing mechanism whatsoever. The directed level becomes trivial for regular dynamics. In fact, both functorial levels must be considered simultaneously to decode the underlying operative mechanisms.

The functorial touchstone for chaos is the existence of multiple, non-equivalent generatex classes. The structural basis for sensitive dependence on initial conditions is algebraically encoded in the alternation between bonded and unbonded regions in phase space, inducing pushout diagrams in the category of semigroups.

Another important remark is that identifying the architecture of a particular chaotic dynamics requires more than merely counting the number of functorial invariants. Just as Betti numbers are less informative than explicitly computing the k -hole generators within a cell complex, generatex classes must be structurally located via the top-cells forming them for their role to be clear.

Because the templex is constructed by processing any dynamical evolution as a point cloud, one can use the

full set of invariants for the intercomparison of datasets, the cross-validation of models, and the benchmarking of simulated outputs against physical observations. In applications, one must work out a dictionary of the concrete meaning of the functorial invariants in terms of the specific problem.

It is also important to stress that the topological definition of chaos that results from this formalism is applicable to finite-time datasets, independently of whether they are obtained from numerical integrations of well-known chaotic systems, from higher-dimensional models as in the climate example or from experimental time series as in the voice production case.

The speech example constitutes the first templex constructed from a fully experimental signal and the first application of the functorial formulation to voice dynamics. The resulting directed invariants provide an operational signature of chaos in voiced sound production that remained undetectable by homologies alone. Chaotic signals in voice production can arise from disparate physiological mechanisms [38]. Because clinical practice frequently conflates structurally distinct nonlinear phenomena under generic perceptual terms like diplophonia or roughness, functorial invariants offer a rigorous tool for disambiguation. Future research applying TMV decompositions to empirical acoustic data from distinct clinical cohorts could reveal whether specific laryngeal pathologies impose unique topological signatures, ultimately enabling diagnosis through non-invasive acoustic recordings. On the other hand, the change from a voiced vowel to an unvoiced sound should translate into a global topological reconfiguration.

The climatic example shows how the formalism works with a four-dimensional phase space and nonautonomous settings. Functorial invariants are of immense value in providing a rigorous topological perspective on broad dynamical concepts such as bifurcations or tipping points [3], weather regimes [39] or extreme events [40]. Topological tipping occurs at those instants when the set of avail-

able generatex classes changes, thus providing a full topological interpretation of such transitions. As discussed in Ref. [41], ensemble realizations of a chaotic system lead to the coexistence of several TMVs at a single instant, offering a topological counterpart to the changes in statistical moments driven by time-dependent forcing [42]. In the context of the large-scale ocean circulation, these directed invariants capture the spontaneous reorganization of mass transport pathways, such as abrupt shifts in the separation of western boundary currents or transitions between distinct gyre regimes. Topological tipping thus encodes the switching of the ocean dynamics between structurally different, physically realizable states. Topological tipping points defined in the context of random attractors with a random tempex require an extension of this formalism to noise-driven chaotic dynamics which is out of the scope of this work [35, 43].

Ultimately, the functorial framework developed here provides a theoretical cornerstone to advance physics-informed machine learning. Traditional dimensionality reduction techniques, such as Principal Component Analysis or Empirical Orthogonal Decompositions, rely on projections that optimize variance but do not guarantee the preservation of the undirected and directed topology of the data. Similarly, while complex network ap-

proaches to time series analysis successfully capture sequential transitions, they often lack the formal topological scaffold required to define robust invariants. The architecture and cost functions of a data-driven model can be validated, or actively guided, based on their capacity to reproduce the generatex semigroup and bond structure of the original system or dataset.

To conclude, this article presents a functorial formulation for chaos topology from data. Placing the tempex within the broader mathematical framework of category theory discloses why homology must not be replaced by directed homology, what kind of object the tempex is, and why two related but distinct functorial chains are required to translate finite-time dynamics into a complete set of topological invariants. This contribution brings together — while keeping them distinct — two notions that are traditionally difficult to reconcile: time and structure.

Acknowledgments The author wishes to thank Michael Ghil and Pablo Amster for careful reading and insightful discussions, and Christophe Letellier for several exchanges on templates. Funds from the ANR project TeM-Plex ANR-23-CE56-0002 are acknowledged.

-
- [1] S. L. Brunton, B. R. Noack, and P. Koumoutsakos, Annual review of fluid mechanics **52**, 477 (2020).
- [2] R. Gilmore, Rev. Mod. Phys. **4**, 1455 (1998).
- [3] M. Ghil and D. Sciamarella, Nonlinear Processes in Geophysics **30**, 399 (2023).
- [4] C. Letellier and V. Messenger, International Journal of Bifurcation and Chaos **20**, 3585 (2010).
- [5] R. Gilmore and M. Lefranc, *The Topology of Chaos: Alice in Stretch and Squeezeland* (John Wiley & Sons, 2012).
- [6] G. E. Karniadakis, I. G. Kevrekidis, L. Lu, P. Perdikaris, S. Wang, and L. Yang, Nature Reviews Physics **3**, 422 (2021).
- [7] J. S. Birman and R. F. Williams, Topology **22**, 47 (1983).
- [8] M. Lefranc, Physical Review E—Statistical, Nonlinear, and Soft Matter Physics **74**, 035202 (2006).
- [9] S. Mangiarotti *et al.*, Habilitation to direct Recherches, Université de Toulouse **3** (2014).
- [10] L. C. Kinsey, *Topology of Surfaces* (Springer Science & Business Media, 2012).
- [11] D. Sciamarella and G. B. Mindlin, Phys. Rev. Lett. **82**, 1450 (1999).
- [12] D. Sciamarella and G. B. Mindlin, Phys. Rev. E **64**, 036209 (2001).
- [13] G. D. Charó, G. Artana, and D. Sciamarella, Phys. D **405**, 132371 (2020).
- [14] M. Grandis, Cahiers de Topologie et Géométrie Différentielle Catégoriques **44**, 281 (2003).
- [15] E. Goubault, in *Proceedings of the Workshop on Geometry and Topology in Concurrency Theory*, Vol. 81 (Electronic Notes in Theoretical Computer Science, 2003) pp. 1–39.
- [16] P. Gaucher, Mathematical Structures in Computer Science **15**, 409 (2005).
- [17] M. Grandis, *Directed Algebraic Topology: Models of Non-Reversible Worlds*, New Mathematical Monographs, Vol. 13 (Cambridge University Press, Cambridge, 2009).
- [18] G. D. Charó, C. Letellier, and D. Sciamarella, Chaos: An Interdisciplinary Journal of Nonlinear Science **32**, 083108 (2022).
- [19] D. Sciamarella and G. D. Charó, in *Topological Methods for Delay and Ordinary Differential Equations: With Applications to Continuum Mechanics* (Springer, 2024) pp. 191–211.
- [20] C. Mosto, G. D. Charó, C. Letellier, and D. Sciamarella, Chaos: An Interdisciplinary Journal of Nonlinear Science **34** (2024).
- [21] Y. Zou, R. V. Donner, N. Marwan, J. F. Donges, and J. Kurths, Physics Reports **787**, 1 (2019).
- [22] J. H. C. Whitehead, Bulletin of the American Mathematical Society **55**, 213 (1949).
- [23] D. Sciamarella, Tempex: A bridge between homologies and templates for chaotic attractors, Wolfram Community, STAFF PICKS (2023), accessed: 2023-12-07.
- [24] S. Eilenberg and S. Mac Lane, Transactions of the American Mathematical Society **58**, 231 (1945).
- [25] S. Mac Lane, *Categories for the Working Mathematician*, Graduate Texts in Mathematics, Vol. 5 (Springer, 1971).
- [26] E. N. Lorenz, J. Atmos. Sci. **20**, 130 (1963).
- [27] O. E. RöSSLer, Physics Letters A **57**, 397 (1976).
- [28] G. D. Charó, D. Sciamarella, J. Ruiz, S. Pierini, and M. Ghil, Chaos: An Interdisciplinary Journal of Nonlinear Science **XX** (2025).
- [29] G. D. Charó, G. Artana, and D. Sciamarella, J. Fluid Mech. **923**, A17 (2021).

- [30] H. Edelsbrunner and J. L. Harer, American Mathematical Society (2010), see Chapter III for Čech and Vietoris–Rips complexes.
- [31] J. R. Munkres, *Elements of Algebraic Topology* (Addison-Wesley, 1984).
- [32] U. Bauer, D. Hien, O. Junge, and K. Mischaikow, arXiv preprint arXiv:2312.04734 (2023).
- [33] S. G. H. Philander, *El Niño and the Southern Oscillation*. (Academic Press, New York, 1990).
- [34] M. Ghil and V. Lucarini, *Reviews of Modern Physics* **92**, 035002 (2020).
- [35] G. D. Charó, M. D. Chekroun, D. Sciamarella, and M. Ghil, *Chaos: An Interdisciplinary Journal of Nonlinear Science* **31**, 103115 (2021).
- [36] S. Pierini and M. Ghil, *Sci. Rep.* **11**, 1 (2021).
- [37] P. Ashwin, U. Feudel, M. Ghil, K. Lehnertz, J.-P. Ortega, and M. Rasmussen, *Chaos: An Interdisciplinary Journal of Nonlinear Science* **36** (2026).
- [38] J. G. Švec and Z. Zhang, *Philosophical Transactions of the Royal Society B* **380**, 20240018 (2025).
- [39] K. Strommen, M. Chantry, J. Dorrington, and N. Otter, *Climate Dynamics* **60**, 1415 (2023).
- [40] C. Letellier, L. Kamdjeu Kengne, M. Zhao, and L. Minnati, *Chaos: An Interdisciplinary Journal of Nonlinear Science* **35** (2025).
- [41] D. Crisan, S. Galatolo, M. Ghil, S. Pierini, D. Sciamarella, and T. Tél, *Chaos: An Interdisciplinary Journal of Nonlinear Science* **36**, 040403 (2026).
- [42] B. Maraldi, H. A. Dijkstra, and M. Ghil, *Chaos: An Interdisciplinary Journal of Nonlinear Science* **35**, 10.1063/5.0253103 (2025).
- [43] G. D. Charó, M. Ghil, and D. Sciamarella, *Chaos: An Interdisciplinary Journal of Nonlinear Science* **33** (2023).